Research Article Vol. 56, No. 35 / December 10 2017 / Applied Optics 9735

applied optics

Focusing anomalies with binary diffractive optical elements

O. Bouzid,[1,2] S. Haddadi,[1,3] M. Fromager,[1] E. Cagniot,[1] K. Ferria,[2] A. Forbes,[4] and K. Ait-Ameur[1,*]

[1]Centre de Recherche sur les Ions, les Matériaux et la Photonique (CIMAP), UMR 6252 CEA-CNRS-ENSICAEN-Université de Caen, 6 Bd Maréchal Juin, 14050 Caen cedex 4, France
[2]Institut d'Optique et Mécanique de Précision, Laboratoire d'Optique Appliquée, Université Ferhat Abbas, Av. Said Boukhraissa, Maabouda 19000 Sétif, Algeria
[3]Faculté de Physique, Université des Sciences et de la Technologie Houari Boumédiène, B.P. N°32, El Alia, Algiers 16111, Algeria
[4]School of Physics, University of the Witwatersrand, Private Bag 3, Johannesburg 2050, South Africa
*Corresponding author: kamel.aitameur@ensicaen.fr

Received 28 August 2017; revised 1 November 2017; accepted 2 November 2017; posted 6 November 2017 (Doc. ID 305641); published 8 December 2017

Binary diffractive optics have been extensively studied to date as tools for arbitrary laser beam shaping and experimentally implemented with etched transparent optics and spatial light modulators. Here we demonstrate that a simple one-step binary optic is able to enhance the intensity of a focused beam, displaying some counter-intuitive focusing anomalies. We explain these effects by considering the optical aberrations in binary diffractive optics and outline how this may be exploited for further improvements in refractive/diffractive combinations for super-resolution microscopy.

OCIS codes: (260.1960) Diffraction theory; (090.1970) Diffractive optics; (090.1000) Aberration compensation; (220.3620) Lens system design.

https://doi.org/10.1364/AO.56.009735

1. INTRODUCTION

Binary diffractive optical elements (DOEs) have found many applications, from diffractive lens and gratings through to general laser beam shaping, and have been extensively reviewed [1,2]. One of the simplest binary DOEs that one can conceive of is a circular phase-aperture (CPA) with a simple step profile in phase, as illustrated in Fig. 1(a). Such elements were first made as simple but tuneable Gaussian to flat-top beam converters [3] and were later found to have unique propagation effects on the transformed beam, e.g., producing optical bottle beams [4]. The advantage of combining refractive and diffractive optics has been understood for some time, particularly for dispersion control [5], compactness [6], and anti-reflection coating with a structured surface [7]. In particular, diffractive and refractive lenses have been combined to produce lower spherical aberration and chromatic aberration in control of white light fields [8].

Here we revisit this venerable subject and demonstrate a counterintuitive example that a simple CPA can enhance the focusing properties of a conventional lens, producing a higher on-axis intensity, even when the overall transmission through the lens is lower. We achieve this by combining a CPA with a variable aperture, exploiting simultaneous diffraction by phase and amplitude, and explain the effects by providing a generalized approach to the study of the optical aberrations of binary diffractive optical elements. These results will be of interest to optical systems engineers who exploit diffractive/refractive control of light in the presence of limiting apertures, as well as to the imaging and microscopy community, where localized fields are known to enhance resolution.

2. CONCEPT

In this paper, we will consider the diffraction properties of a simple binary DOE, illustrated in Fig. 1(a), and characterized by the following complex transmittance:

$$\tau(\rho) = \begin{cases} +1 & \text{for } \rho < \rho_0 \\ -1 & \text{for } \rho \geq \rho_0 \end{cases}, \tag{1}$$

where ρ is the radial coordinate, and ρ_0 is the radius of the phase step.

With *a priori* knowledge of the outcome, we are able to consider the scenario in Fig. 1(b): rather than focussing with a simple lens, we combine refraction with amplitude (variable aperture) and phase (CPA) diffraction effects, and illustrate some propagation anomalies, including an enhancement in focussing properties, namely, an increase in the maximum of on-axis intensity after the lens as compared to only a lens present.

In the configuration shown in Fig. 1(b) the CPA and aperture (of diameter $2\rho_D$) are assumed to be placed arbitrarily close

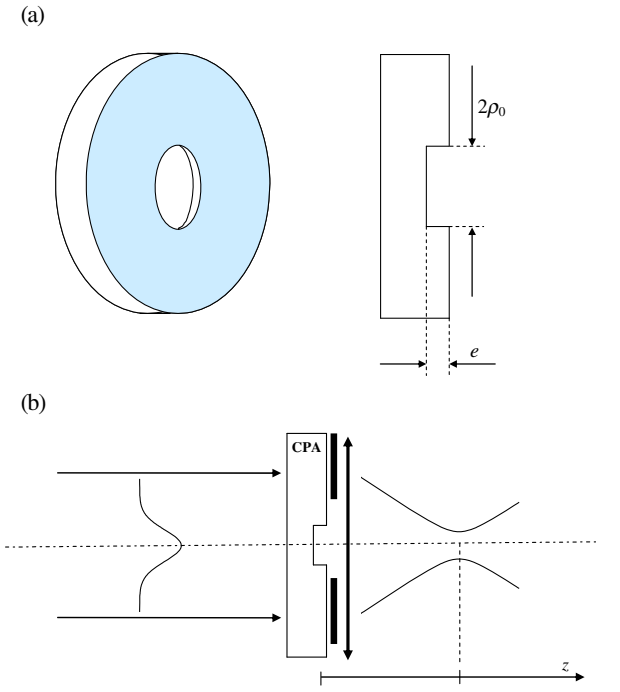

Fig. 1. (a) Schematic layout showing the circular phase aperture (CPA) made of a transparent plate with a relief of depth $e = \lambda[2(n-1]$ where n denotes the refractive index of the plate. (b) Schematic layout showing the CPA, the aperture, and the focusing lens.

to the lens (of focal length f). Intuitively, one might expect that the focal spot resulting from the focussing of an incoming Gaussian beam (of width W_0) would exhibit a decrease in on-axis intensity as the aperture is closed. In contrast, we demonstrate that for a judicious choice of the relative scale parameters $Y_D = \rho_D/W_0$ and $Y = \rho_0/W_0$, the maximum of on-axis intensity can in fact be increased. We explain and interpret this counterintuitive behavior in terms of *diffractive aberrations* (defocus and spherical aberration) generated by the CPA.

Consider a collimated Gaussian beam of width W_0 incident on the optical setup of Fig. 1(b), whose amplitude distribution is given by

$$E_{\text{in}}(\rho) = E_0 \exp[-\rho^2/W_0^2]. \tag{2}$$

Note that the incoming wavefront described by Eq. (2) is flat, but at the lens entrance it has a discontinuity due to the phase profile of the CPA. The diffracted field distribution $E_d(r, Z)$ in any plane $Z \gg \lambda$ beyond the lens is given by the Fresnel–Kirchhoff integral,

$$E_d(r,Z) = \frac{2\pi}{\lambda Z}\int_0^{\rho_D} \tau(\rho) E_{\text{in}}(\rho) \times \exp\left\{\frac{i\pi\rho^2}{\lambda}\left(\frac{1}{Z}-\frac{1}{f}\right)\right\} J_0\left(\frac{2\pi}{\lambda Z} r\rho\right)\rho \mathrm{d}\rho, \tag{3}$$

where r is the radial coordinate in the plane observation Z, $k = 2\pi/\lambda$ is the wave number, and J_0 is the zero-order Bessel function of first kind. In the following, we will consider the on-axis intensity distribution $I_d(0, Z) = |E_d(0, Z)|^2$. One can show that the on-axis electrical field $E_d(0, Z)$ may be expressed as

$$E_d(0,Z) = \frac{2\pi W_0^2 E_0}{\lambda Z}\left\{\int_0^Y \exp(-X^2)\exp(iaX^2)X\mathrm{d}X - \int_Y^{Y_D} \exp(-X^2)\exp(iaX^2)X\mathrm{d}X\right\}, \tag{4}$$

where the reduced transverse coordinate X is defined $X = \rho/W_0$, and the Z dependent parameter a is given by

$$a = \frac{\pi W_0^2}{\lambda}\left[\frac{1}{Z}-\frac{1}{f}\right]. \tag{5}$$

Finally, one easily finds the following expression for the diffracted on-axis intensity at any plane after the lens:

$$I_d(0,Z) = \left(\frac{\pi W_0^2 E_0}{\lambda Z}\right)^2 \cdot \frac{1}{1+a^2}\{1 + 4e^{-2Y^2} - 4e^{-Y^2}\cos(aY^2) + 2e^{-Y_D^2}\cos(aY_D^2) + e^{-2Y_D^2} - 4e^{-(Y^2+Y_D^2)}\cos a(Y_D^2 - Y^2)\}. \tag{6}$$

Another quantity of importance is the transmission through the aperture as a power ratio, given by

$$T_D = 1 - \exp[-2Y_D^2]. \tag{7}$$

The variation of the maximum value of the on-axis intensity $I_d(0, Z)$ versus the parameter Y_D is shown in Fig. 2. For more clarity, Figs. 2(b) and 2(c) display the variations of the maximum value of $I_d(0, Z)$ versus the diaphragm parameter Y_D for two values of Y. For $Y = 0.2$, we find the expected result that the maximum intensity on the optical axis reduces as the aperture is closed, i.e., as Y_D decreases. In contrast, we can clearly recognize that one observes a stronger focus when closing the aperture over a certain range of Y_D values (1.7 to 1.8). Comparing the peak on-axis intensity for $Y_D \sim 1.7$ and $Y_D > 3$ (i.e., without aperture) shows that the maximum intensity has been enhanced by just more than 10% while still maintaining a good energy transmission of $T_D > 99\%$. It is observed that for $Y < 0.5$ and $Y > 1.9$, the peak value of the on-axis intensity decreases as the aperture is closed. While the increase of the peak of on-axis intensity is a modest advance, it does illustrate an interesting optical phenomenon that appears at first counterintuitive, and which we will address in the next section.

Another characteristic of the focused beam is the axial position of the focus point. It is known that when a Gaussian beam is focused by a hard-apertured lens that the point of the maximum on-axis intensity is not at the geometric focus $Z = f$ but is shifted toward the apertured lens. This effect is referred to as the focal shift and has been thoroughly studied in the 1980s [9–13] but is less known for hybrid systems such as that investigated here. It is convenient to describe this effect by the *relative focal shift* (RFS) expressed by the quantity $(Z_{\max} - f)/f$, where $Z_{\max}$ is the axial distance between the lens and the position of the maximum on-axis intensity. The variation of this shift is shown in Fig. 3(a) as a function of Y for the limiting case $Y_D \to \infty$ (without the diaphragm) and as a function of Y_D (without the CPA). The relative focal shift is in both cases always negative and tends to vanish for high values of Y and Y_D. For small values of Y and Y_D, the behavior is very different, since it vanishes for $Y \to 0$ while it is maximum in absolute value when Y_D becomes very small.

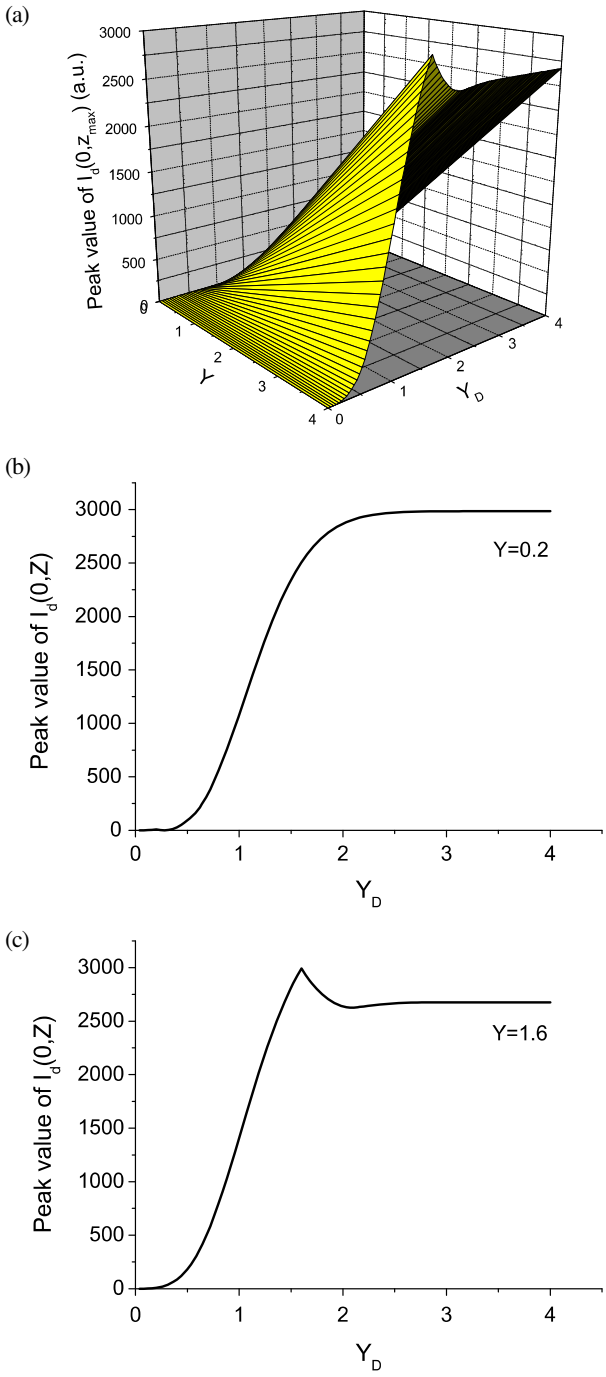

Fig. 2. (a) Variation in the maximum value of the on-axis intensity as a function of the aperture and CPA normalized diameters. Note that the maximum does not occur at the same distance after the lens. (b) and (c) show two cross sections for $Y = 0.2$ and $Y = 1.6$, respectively.

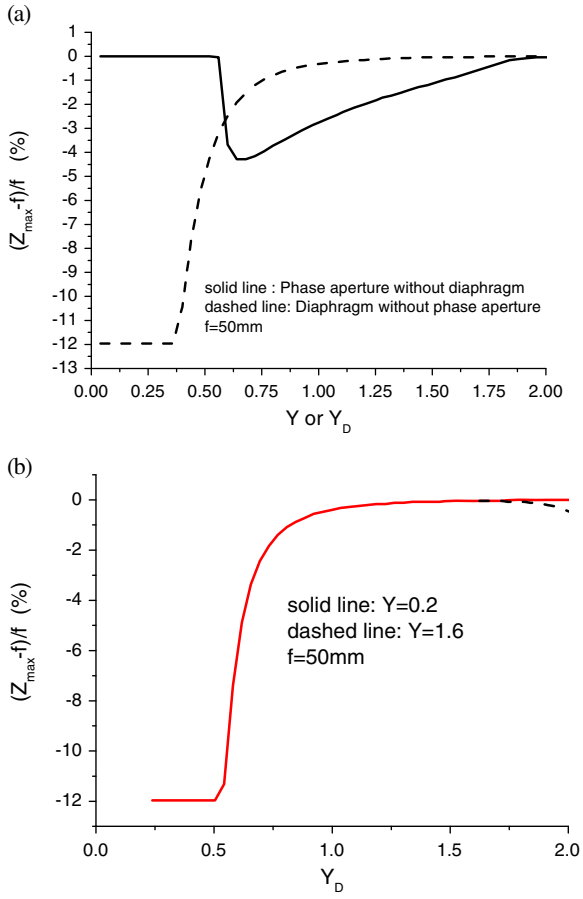

Fig. 3. (a) Variations of the relative focal shift $(Z_{\max} - f)/f$ as a function of the aperture and CPA normalized diameters. (b) Variations of the relative focal shift $(Z_{\max} - f)/f$ as a function of Y_D for two values of Y (solid line: $Y = 0.2$, dashed line: $Y = 1.6$).

Figure 3(b) shows the variation of the focal shift when both the diaphragm and CPA are present, using parameters of $Y = 0.2$ and 1.6 as examples. The plot suggests that the hard-aperture effect dominates the process.

With this in mind, we can now return to the previously discussed effect of the maximum on-axis intensity *increasing* when introducing a *decreasing* aperture diameter. We can speculate about the origin of this effect by considering the aberrations resulting from the wavefront distortion due to the CPA. Indeed, it is well known that focusing a laser beam by a lens with spherical aberration leads to a lower intensity in the focal point compared to aberration-free focusing [14,15]. However, when the lens is hard apertured, it can result in a stronger focus [16]. This is not the only argument that suggests interest in the aberrations induced by the circular phase aperture. Indeed, the typical laser Gaussian beam reshaping achieved by a CPA, namely the flat-top and the optical bottle beam, are also observable with the spherical aberration [17–19]. Moreover, the RFS effect discussed above could be connected to the diffractive lensing effect [20,21] attached to the CPA, which could be described in term of *defocus* as it will be seen hereafter. Thus it is pertinent to consider the effective aberrations of the CPA, which we will describe in terms of Zernike polynomials in the section to follow.

3. DIFFRACTIVE ABERRATIONS

As pointed out in Section 1, the incident Gaussian beam passing through the CPA will have its wavefront degraded by the phase discontinuity described by Eq. (1). As a consequence, one can expect that the CPA induces optical aberrations.

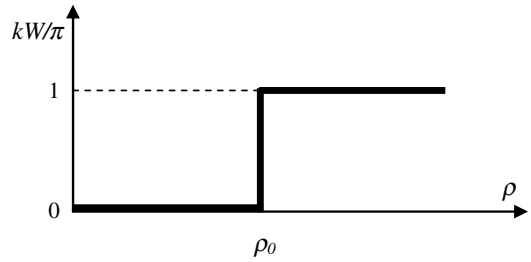

Fig. 4. Transverse profile of the wave aberration function associated with the CPA.

For determining the latter, we will assume an incident plane wavefront beam on the CPA so that the transmission function of the CPA is $\exp[ikW(\rho,\theta)]$. The evolution of the phase kW versus the radial coordinate ρ is shown in Fig. 4 for the CPA.

As usual, the phase is expanded as a linear combination of Zernike polynomials, Z_j, as follows:

$$W(\bar{\rho},\theta)=\sum_{j=1}^{\infty}a_jZ_j(\bar{\rho},\theta), \tag{8}$$

where the index j is a polynomial-ordering number, and a_j are the expansion or aberration coefficients. The normalized radial coordinate $\bar{\rho}$ is defined as $\bar{\rho}=\rho/(2W_0)$. Note that the circle of radius $2W_0$ contains 99.96% of the incident power as we use this to define the unit circle for the Zernike polynomials $Z_j(\bar{\rho},\theta)$ to ensure their orthogonality, i.e., $(0\le\bar{\rho}\le 1)$. With this approach, one can view the situation as follows: the aperture, which may be of any size, truncates the incoming Gaussian beam. This truncated beam is then influenced by the aberrations defined using the original beam diameter as the unit circle. Note that this definition does not affect the physics of the situation, and so while rescaling would affect the values of the aberrations it would not affect the trends nor the outcomes. Moreover, this approach allows us to separate the beam profile from the aberration definition. If so desired, the reader may alter this to renormalize the aberration coefficients by taking into account the profile of the truncated beam [22–25]. Thus we can compute the coefficients a_j as the projections (i.e., inner product) of the wave aberration function on each basis function as follows:

$$a_j=\frac{1}{\pi}\int_0^1\int_0^{2\pi}W(\bar{\rho},\theta)Z_j(\bar{\rho},\theta)\bar{\rho}\,\mathrm{d}\bar{\rho}\,\mathrm{d}\theta. \tag{9}$$

We use the dimensionless coefficients

$$A_j=\frac{a_j}{\lambda}, \tag{10}$$

in order to have an efficient description of the wavefront aberration in terms of the number of wavelengths. In principle, the sum in Eq. (8) is infinite, but it is usually truncated after a finite number of terms accurately describe the field. Here we work with polynomials up to index $j=37$. Some example polynomials are given in Table 1, with full details found elsewhere [22].

Because of the rotational symmetry of the CPA, most of the coefficients a_j are equal to zero except for five of them: A_1, A_4, A_{11}, A_{22}, and A_{37}. Table 1 gives the corresponding Zernike polynomials and the associated aberration. Note that the aberration term for $j=4$ corresponds to defocus, i.e., a pure lensing effect, which gives rise to the focal shift.

Table 1. Some Example Zernike Polynomials

j	Z_j	Type of Aberration
1	1	**Piston**
4	$\sqrt{3}(2\bar{\rho}^2-1)$	**Defocus**
11	$\sqrt{5}(6\bar{\rho}^4-6\bar{\rho}^2+1)$	**Primary spherical**
22	$\sqrt{7}(20\bar{\rho}^6-30\bar{\rho}^4+12\bar{\rho}^2-1)$	**Secondary spherical**
37	$3(70\bar{\rho}^8-140\bar{\rho}^6+90\bar{\rho}^4-20\bar{\rho}^2+1)$	**Tertiary spherical**

The calculation of Eq. (9) involves the function $F_j(\bar{\rho})$, for $j=1$, 4, 11, 22, and 37, defined as

$$F_j(\bar{\rho})=\int Z_j(\bar{\rho})\bar{\rho}\,\mathrm{d}\bar{\rho}, \tag{11}$$

$$F_1(\bar{\rho})=\bar{\rho}^2/2, \tag{12}$$

$$F_4(\bar{\rho})=\frac{\sqrt{3}}{2}[\bar{\rho}^4-\bar{\rho}^2], \tag{13}$$

$$F_{11}(\bar{\rho})=\sqrt{5}[\bar{\rho}^6-1.5\bar{\rho}^4+0.5\bar{\rho}^2], \tag{14}$$

$$F_{22}(\bar{\rho})=\sqrt{7}[2.5\bar{\rho}^8-5\bar{\rho}^6+3\bar{\rho}^4-0.5\bar{\rho}^2], \tag{15}$$

$$F_{37}(\bar{\rho})=3[7\bar{\rho}^{10}-17.5\bar{\rho}^8+15\bar{\rho}^6-5\bar{\rho}^4+0.5\bar{\rho}^2]. \tag{16}$$

Note that the phase term $kW(\rho)$ has two possible values: 0 (for $0\le\bar{\rho}<\bar{\rho}_0$) and π (for $\bar{\rho}_0\le\bar{\rho}\le 1$). This results in a reduced aberration coefficient, A_j, following

$$A_j=\{F_j(1)-F_j(\bar{\rho}_0)\}=-F_j(\bar{\rho}_0), \tag{17}$$

where $\bar{\rho}_0=\rho_0/(2W_0)$. The plots in Fig. 5 display the variations of the coefficients A_j excluding the piston coefficient, A_1, as this does not constitute an aberration [23] and therefore has a little interest in this study. It is seen that the different orders of spherical aberration (A_{11}, A_{22}, A_{37}) oscillate with about the same amplitude as the radius of the CPA is varied.

Before proceeding, it is important to note that the plots displayed in Fig. 5 cannot be directly confirmed experimentally by using the usual Shack–Hartman sensor, as this device is intrinsically insensitive to phase discontinuities. However, the

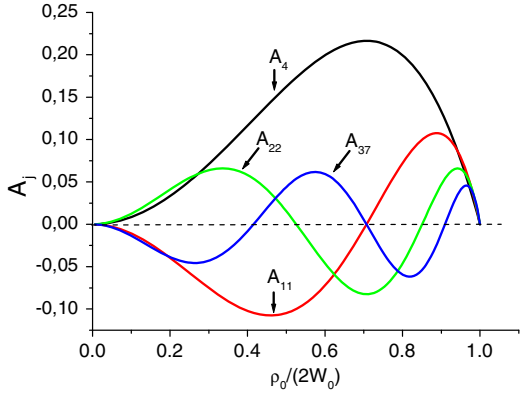

Fig. 5. Variations of the aberration coefficients A_j versus the CPA normalized radius.

reconstruction of the wavefront is possible using a method based on modal decomposition by computer-generated holograms [26].

Let us now focus on the focal length, f_{eq}, which characterizes the diffractive lensing associated with the CPA but without the aperture effect. For that, let us first discuss the equivalent focal length of a pure defocus. It is worth pointing out the phase of a collimated laser beam having passed through a thin lens of focal length f may be written as

$$W_L = \frac{\rho^2}{2f} = \frac{R^2\bar{\rho}^2}{2f}, \tag{18}$$

where $R = 2W_0$ is the radius of the Zernike circle. The only non-zero aberration coefficient a_4 can be obtained by resolving the following integral given by Eq. (9),

$$a_4 = \frac{1}{\pi}\int_0^1\int_0^{2\pi} W_L(\bar{\rho},\theta)Z_4(\bar{\rho},\theta)\bar{\rho}\,\mathrm{d}\bar{\rho}\,\mathrm{d}\theta,$$

$$a_4 = \frac{1}{\pi}\int_0^{2\pi}\mathrm{d}\theta\int_0^1 \frac{R^2\bar{\rho}^2}{2f}\bar{\rho}\sqrt{3}(2\bar{\rho}^2-1)\mathrm{d}\bar{\rho},$$

finally reducing to

$$a_4 = \frac{\sqrt{3}R^2}{12f}. \tag{19}$$

Consequently, if we are dealing with a pure defocus aberration characterized by the normalized coefficient $A_4 = a_4/\lambda$, then, taking into account Eq. (19), it is equivalent to a pure lens having the focal length f_{eq} given by

$$f_{eq} = \frac{\sqrt{3}R^2}{12\lambda A_4}. \tag{20}$$

The position z_m of the new focus is given by

$$\frac{1}{z_m} = \frac{1}{f} + \frac{1}{f_{eq}}, \tag{21}$$

which leads to the relative focal shift $(z_m - f)/f$ given in Fig. 6.

It is worth noting that in Fig. 6 the CPA effect is described in terms of a pure lens. The comparison between the relative focal shift in Fig. 3 without the aperture and that in Fig. 6 shows that the agreement is only qualitative. This can be understood since besides its diffractive lensing effect, the CPA also has an effect on the beam shaping [2,3], as is shown in Fig. 7. This reshaping action has, for instance, a tendency to move energy from the axis to off-axis regions, thus also affecting the position of the maximum on-axis intensity.

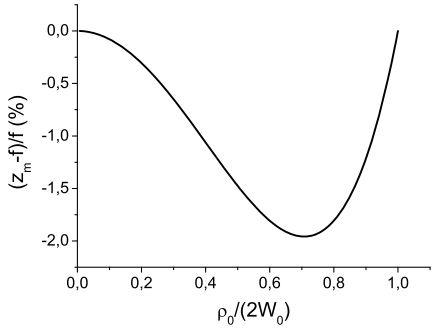

Fig. 6. Variations of the relative focal shift determined from the defocus term of the aberration associated with the circular phase aperture of radius ρ_0; W_0 is the radius of the collimated incident Gaussian beam.

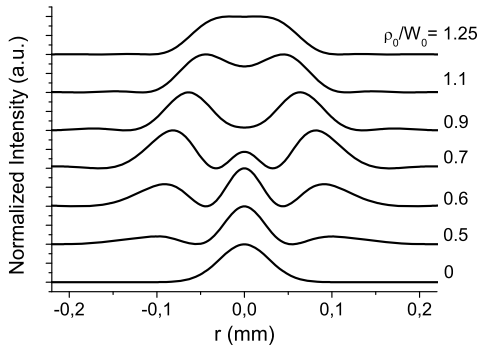

Fig. 7. Normalized intensity distribution $I_d(r, f)$ in the focal plane of the lens, showing the ability of the CPA to reshape an incident Gaussian beam into a flat-top profile, a doughnut profile, or an LG_{10}-shaped profile.

4. MULTI-RINGED STRUCTURES

We can wonder about the possibility to increase the generated aberrations when the phase plate is made up of several concentric phase discontinuities (0 – π – 0 – π – …). Note that such devices are particularly useful for extending the depth of focus of a laser beam [27–32]. This property, often called as *axial super-resolution*, is useful in some applications such as optical tweezers, optical data storage, fluorescent imaging, and harmonic generation. Here we consider a binary concentric phase mask made up of N zones of phase $\varphi = \pi$. The zones $\varphi = \pi$ and $\varphi = 0$ are assumed to all have the same width. The phase of each ring is set alternately equal to 0 or π, and the number of zones N varies from 1 to 6. Figure 8 shows an example for $N = 3$.

The resulting aberration coefficients may easily be found by applying Eq. (9), from which we find

$$A_j = \sum_{i=1}^{N-1} F_j(\bar{\rho}_{2i}) - \sum_{i=1}^{N} F_j(\bar{\rho}_{2i-1}), \tag{22}$$

where $\{\bar{\rho}_{2i}\}$ are the radii of the rings for which the phase change is $(\pi \to 0)$, and $\{\bar{\rho}_{2i-1}\}$ are the radii of the rings for the phase change $(0 \to \pi)$. Table 2 displays the defocus coefficient A_4,

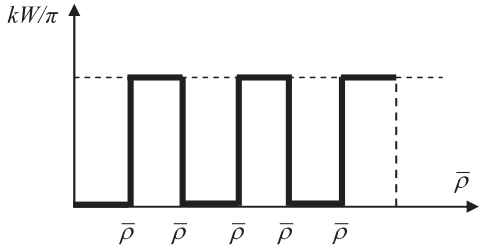

Fig. 8. Variations of the normalized wave aberration function kW/π versus the normalized radial coordinate for a binary concentric phase mask for $N = 3$.

Table 2. Aberration Coefficients of a Binary Concentric Phase Mask Made Up of N Zones of Phase $\varphi = \pi$[a]

N	A_4	A_{11}	A_{22}	A_{37}
1	16.23×10^{-2}	-10.48×10^{-2}	1.55×10^{-2}	$\mathbf{4.39 \times 10^{-2}}$
2	10.14×10^{-2}	8.18×10^{-2}	-3.57×10^{-2}	$\mathbf{-12.26 \times 10^{-2}}$
3	7×10^{-2}	7.57×10^{-2}	3.95×10^{-2}	$\mathbf{-4.14 \times 10^{-2}}$
4	5.32×10^{-2}	6.23×10^{-2}	5.12×10^{-2}	$\mathbf{1.016 \times 10^{-2}}$
5	4.28×10^{-2}	5.20×10^{-2}	4.96×10^{-2}	$\mathbf{2.88 \times 10^{-2}}$
6	$\mathbf{3.58 \times 10^{-2}}$	$\mathbf{4.43 \times 10^{-2}}$	$\mathbf{4.54 \times 10^{-2}}$	$\mathbf{3.45 \times 10^{-2}}$

[a]The zones $\varphi = \pi$ and $\varphi = 0$ are assumed to all have the same width.

the primary spherical aberration coefficient A_{11}, and the higher-order spherical aberration coefficients A_{22} and A_{37}. Note that the case $N = 1$ corresponds to the CPA already studied earlier. Contrary to what could be expected, we find (see Table 2) that the aberration coefficients do not increase with the number of dephasing zones; it is in fact exactly the contrary.

For the particular application given above, namely, the extension of depth of focus, the sizes of the zones are determined using the standard optimization process [29] (genetic/annealing). It is interesting to determine the aberration coefficients of the three -zones of the phase $\varphi = \pi$ mask used in [25], for which it has been observed that the depth of focus increased by a factor of 16. Using the six values of the radius at which the phase changes from 0 to π or π to 0 given in [29], we obtain the following: $A_4 = 19.09 \times 10^{-2}$, $A_{11} = -3.53 \times 10^{-2}$, $A_{22} = 5.54 \times 10^{-2}$, and $A_{37} = 1.19 \times 10^{-3}$. Note that in [29] the zones have unequal widths, unlike the case considered in Table 2. We can notice that the tertiary spherical aberration coefficient A_{37} in Eq. (23) is ten times lower than A_{11} and A_{22}. This implies that it probably could be conceivable, at the price of cumbersome calculations, to design a phase plate taking the form of a binary concentric phase mask for the generation of given primary, secondary, and tertiary spherical aberrations by using standard optimization process (genetic/annealing) for retrieving the optimal zone radii as well as their number. If this could be possible, one could envisage the fabrication of a pure-phase apodizer without resorting to a continuous surface-relief profile, the latter being more complicated to fabricate and more expensive than a binary optic that requires only one etching level. Note that the peculiarity of a binary concentric phase mask is to generate not only defocus and primary spherical aberration, but also high-order spherical aberrations, and this is probably the reason for why the depth of focus can be increased by a large factor of 16 times [29]. Indeed, it is known that focusing a Gaussian beam with a lens made entirely of a quartic phase mask (primary spherical aberration) only allows a moderate increase in the depth of focus of about 3 times [33,34].

5. CONCLUSION

In this paper, we have shown how a simple binary diffractive optical element that, together with an aperture and lens, results in enhanced focusing. We explain this by a careful analysis of the aberrations (defocus, primary, and high-order spherical aberration) generated by DOE. The peculiarity of this device is that it generates spherical aberration (primary, secondary, and tertiary) that oscillates with the circular phase aperture radius. We have also characterized the aberrations' coefficients of a binary diffractive optical element made up of wrapped dephasing zones ($0 - \pi - 0 - \pi - 0 - \pi \ldots$). Globally, it is found that the value of the aberration coefficients reduces as the number of zones increases. This behavior can be exploited for extending the depth of focus of a laser beam, creating thus super-resolution fields. It is probably possible to design a phase plate with wrapped dephasing zones of unequal widths for the generation of a given primary, secondary, and tertiary spherical aberration. If this could be carried out, one can envisage the fabrication of a pure-phase apodizer without exploiting a continuous surface-relief profile, which is more complicated and expensive than a binary optics, requiring only one etching level.

REFERENCES

1. D. C. O'Shea, T. J. Suleski, A. D. Kathman, and D. W. Prather, *Diffractive Optics: Design, Fabrication and Test* (SPIE, 2004).
2. J. Turunen and F. Wyrowski, *Diffractive Optics for Industrial and Commercial Applications* (Wiley, 1998).
3. R. Bourouis, K. Aït-Ameur, and H. Ladjouze, "Optimization of the Gaussian beam flattening using a phase-plate," J. Mod. Opt. **44**, 1417–1427 (1997).
4. A. Harfouche, B. Boubaha, M. Fromager, and K. Aït-Ameur, "Comparison between interferometric and diffractive laser beam shaping," J. Opt. **16**, 125712 (2014).
5. M. Bass, *Handbook of Optics*, 3rd ed. (Mc Graw-Hill, 2010), Vol. **I**, Chap. 23.
6. N. Yu and F. Capusso, "Flat optics with designer metasurfaces," Nat. Mater. **13**, 139–150 (2014).
7. C. David, P. Häberling, M. Schnieper, J. Söchtig, and C. Zschokke, "Nano-structured anti-reflective surfaces replicated by hot embossing," Microelectron. Eng. **61**–62, 435–440 (2002).
8. A. Flores, M. R. Wang, and J. J. Yang, "Achromatic hybrid refractive-diffractive lens with extended depth of focus," Appl. Opt. **43**, 5618–5630 (2004).
9. Y. Li and E. Wolf, "Focal shifts in diffracted converging spherical waves," Opt. Commun. **39**, 211–215 (1981).
10. Y. Li and E. Wolf, "Focal shift in focused truncated Gaussian beam," Opt. Commun. **42**, 151–156 (1982).
11. Y. Li, "Dependence of the focal shift on Fresnel number and f number," J. Opt. Soc. Am. **72**, 770–774 (1982).
12. M. P. Givens, "Focal shifts in diffracted converging spherical waves," Opt. Commun. **41**, 145–148 (1982).
13. V. N. Mahajan, "Axial irradiance and optimum focusing of laser beams," Appl. Opt. **22**, 3042–3053 (1983).
14. A. Yoshida and T. Asakura, "Propagation and focusing of Gaussian laser beams beyond conventional diffraction limit," Opt. Commun. **123**, 694–704 (1996).
15. J. Pu and H. Zhang, "Intensity distribution of Gaussian beams focused by a lens with spherical aberration," Opt. Commun. **151**, 331–338 (1998).
16. G. P. Karman, A. V. Duijl, and J. P. Woerdman, "Observation of a stronger focus due to spherical aberration," J. Mod. Opt. **45**, 2513–2517 (1998).
17. J. A. MacAndrew, M. R. Humphries, W. T. Welford, and J. A. Golby, "A beam shaping system," Proc. SPIE **1500**, 172–176 (1991).
18. A. A. Alkelly, "Spot size and radial intensity distribution of focused Gaussian beams in spherical and non-spherical aberration lenses," Opt. Commun. **277**, 397–405 (2007).
19. D. M. Karnakis, J. Fieret, P. T. Rumsby, and M. C. Gower, "Microhole drilling using reshaped pulsed Gaussian laser beams," Proc. SPIE **4443**, 150–158 (2001).
20. E. Cagniot, M. Fromager, T. Godin, N. Passilly, and K. Aït-Ameur, "Transverse superresolution technique involving rectified Laguerre-Gaussian LG_p^0 beams," J. Opt. Soc. Am. A **28**, 1709–1715 (2011).
21. R. R. Letfullin and O. A. Zayakin, "Diffractive focusing of a Gaussian beam," J. Russ. Laser Res. **23**, 148–160 (2002).

22. V. N. Mahajan, "Zernike circle polynomials and optical aberrations of system with circular pupils," Appl. Opt. **33**, 8121–8124 (1994).
23. V. N. Mahajan, *Optical Imaging and Aberrations: Part I. Ray Geometrical Optics* (SPIE, 1998), Chap. 3, p. 157.
24. C. Mafusire and A. Forbes, "Generalised beam quality factor of aberrated truncated Gaussian laser beams," J. Opt. Soc. Am. A **28**, 1372–1378 (2011).
25. C. Mafusire and T. P. J. Kruger, "Strehl ratio and amplitude-weighted generalised orthonormal Zernike-based polynomials," Appl. Opt. **56**, 2336–2345 (2017).
26. C. Schulze, D. Naidoo, D. Flamm, O. A. Schmidt, A. Forbes, and M. Duparré, "Wavefront reconstruction by modal decomposition," Opt. Express **20**, 19714–19725 (2012).
27. D. M. de Juana, V. F. Canales, P. J. Valle, and M. P. Cagigal, "Focusing properties of annular phase filters," Opt. Commun. **229**, 71–77 (2004).
28. X. Gao, F. Gan, and W. Xu, "Superresolution by three-zone pure phase plate with 0, π, 0 phase variation," Opt. Laser Technol. **39**, 1074–1080 (2007).
29. Y. Xu, J. Singh, C. J. Sheppard, and N. Chen, "Ultra long high resolution beam by multi-zone rotationally symmetrical complex pupil filter," Opt. Express **15**, 6409–6413 (2007).
30. H. Wang, L. Shi, B. Lukyanchuk, C. Sheppard, and C. Chong, "Creation of a needle of longitudinally polarized light in vacuum using binary optics," Nat. Photonics **2**, 501–505 (2008).
31. L. Liu, F. Diaz, L. Wang, B. Loiseaux, J.-P. Huignard, C. J. Sheppard, and N. Chen, "Superresolution along extended depth of focus with binary-phase filters for the Gaussian beam," J. Opt. Soc. Am. A **25**, 2095–2101 (2008).
32. Z. Nie, G. Shi, X. Zhang, Y. Wang, and Y. Song, "Generation of super-resolution longitudinally polarized beam with ultra-long depth of focus using radially polarized hollow Gaussian beam," Opt. Commun. **331**, 87–93 (2014).
33. X. Liu, X. Cai, S. Chang, and C. P. Grover, "Optical system having a large focal depth for distant object tracking," Opt. Express **11**, 3242–3247 (2003).
34. T. Zao, Y. Chen, W. Zhang, Z. Ye, and F. Yu, "Focal depth extending using rotational symmetric pupil masks," Chin. Opt. Lett. **5**, 71–73 (2007).